EPR Study of the Solid Solutions $Ni_xFe_{1-x}S_2$, $Co_xFe_{1-x}S_2$, and $Co_xNi_yFe_{1-x-y}S_2$†

R. N. Chandler* and R. W. Bené

Department of Electrical Engineering and Electronics Research Center, University of Texas at Austin, Austin, Texas 78712

(Received 5 March 1973)

This paper reports an EPR study of the pyrite solid solutions $Co_xFe_{1-x}S_2$, $Ni_xFe_{1-x}S_2$, and $Co_xNi_yFe_{1-x-y}S_2$. The single-ion spectrum for dilute Ni^{2+} in a pyrite structure was fitted to a spin Hamiltonian of the form $H_s = g_z\mu_B S_z H_z + g_x\mu B(S_xH_x + S_yH_y) + DS_z^2$, where $g_z = 2.13 \pm 0.005$, $g_x = g_y = 2.11 \pm 0.005$, and $D = -1.21$ cm^{-1}. The single-ion spectrum for Co^{2+} in FeS_2 showed evidence of dynamic Jahn-Teller activity, with a broad isotropic line at $g = 2.18 \pm 0.02$. At metallic concentrations, FeS_2:Co displayed the classically asymmetric, isotropic line of a conduction electron but with an unusually high g value of $g = 2.12 \pm 0.005$, indicating the partial ionic character of narrow-band electrons. The system FeS_2:Ni:Co displayed both the broad lines characteristic of the itinerate cobalt e_g electrons and the localized Ni^{2+} spectrum. The peculiar Ni^{2+} line shapes resulting from exchange effects with the itinerate electrons are analyzed on the basis of existing s-d interaction theory.

I. INTRODUCTION

A. General

As a class of compounds, the transition-metal oxides and dichalcogenides have attracted much interest because of their high incidence of electric and magnetic phase transitions within a convenient temperature range (77–400 °K). These materials all share a common property of possessing narrow d-electron bands that often dominate their magnetic and electric behavior. These narrow-band electrons may be described as an intermediate case bounded at one extreme by wide-band electrons described by the Bloch model and at the other by localized Heiter-London electrons. A formal model[1,2] has been proposed for these particles and some qualitative application made on the calculation of susceptibility and conductivity.[3–6] To date, however, there has been little experimental work to support the theory.

A subgroup of this class of materials is the iron group disulfides. This group is particularly appealing to the experimentalist since its $3d$ electrons are free from overlapping wide bands. Moreover, the electrons responsible for magnetic properties are also responsible for conduction, and one can expect changes in magnetic and electric properties to be strongly correlated.

This paper reports on an electron-paramagnetic-resonance (EPR) study of $Ni_xFe_{1-x}S_2$, $Co_xFe_{1-x}S_2$, and $Co_xNi_yFe_{1-x-y}S_2$ in solid solutions. These compounds exhibit transport properties ranging from semiconductor to metal while their magnetic states run from diamagnetic to ferromagnetic and antiferromagnetic.

B. Crystal Preparation

All crystals were grown using a halogen-transport technique described by Bouchard.[7] The pyrites were first grown in polycrystalline form by twice reacting the stoichiometric mixture of sulfur and iron, cobalt, or nickel in an evacuated Vycor tube for 5 days at 680 °C. Initially all polycrystalline samples were tested by x-ray diffraction to ensure a pyrite structure. The polycrystalline material was then placed in a Vycor tube 11 mm in diameter and 10 cm in length, filled with 175–200 torr of chlorine gas and sealed. A Lindberg three-zone furnace was adjusted to supply a gradient of 50–70 °C along the length of the tube with the charged end of the tube hottest at 695 °C.

Crystal morphology was typically pyrite, i.e., predominately cubic with some octahedral crystals and a few pentagonal dodecahedron. In general, the addition of cobalt in the FeS_2 host caused pitting in the crystal faces—a phenomena which proved useful in predetermining whether the doping was successful. The largest crystals were 4 mm on a side and 40 mg in weight, although crystals used in the spectrometer were smaller, around 1 mg in weight and 0.5 mm on a side, to prevent cavity loading. $Co_xFe_{1-x}S_2$ crystals were grown from $x = 0.00005$ to $x = 1.0$. $Ni_xFe_{1-x}S_2$ growth seems to be limited to $x < 0.10$, with the exception of the end point $x = 1$. Our crystals of $Ni_xFe_{1-x}S_2$ covered the range from $x = 0.0004$ to $x = 0.03$.

Crystals were oriented in the spectrometer with respect to one of their equivalent ⟨111⟩ axes. In most cases, where cubic or octahedral morphology was present, the ⟨111⟩ faces could be visually

identified. A few crystals required face identification through x-ray analysis. In these cases a Weissenberg camera was used to display the three-fold rotational symmetry required of all body diagonals.

C. Microwave Spectrometer

Two microwave spectrometers were used in this study; one operating at 35 GHz and another at 24 GHz. The design features on both are identical and of standard construction. The cylindrical cavities operate in the TE_{011} mode and are made of silver-plated copper. The waveguide is of stainless steel to retard heat flow into the Dewar. An electronic AFC circuit locks the klystron on the resonant frequency of the cavity. Phase-sensitive detection is accomplished through the use of a PAR lock-in amplifier. The recent availability of Schottky-barrier diodes has enabled us to improve the signal-to-noise ratio by 10 dB over that obtained using the quietest point-contact devices. The magnetic field is swept automatically from 0 to 15 kOe using a feedback control circuit.

Nonconducting crystals were placed in the center of the cavity supported by a 1-mm quartz rod. For the semimetallic samples normally encountered in this study, we decoupled the crystals from the rf field by lowering them. Metallic samples were placed on the cavity bottom. The highly doped ($x \geq 0.09$) magnetic samples $Co_xFe_{1-x}S_2$ were actually inserted in the cavity bottom to minimize any loading effects on ferromagnetic-resonance line shape. Although the fields at the cavity bottom are quite nonuniform, they should have only a small effect in comparison with the nonuniformity within the sample caused by the skin effect.

D. Determination of Cobalt and Nickel Impurity Concentrations in FeS_2

To determine the doping levels of cobalt and nickel in FeS_2, we relied on nuclear-activation analysis. For the heavier concentrations (near 1 at.%), this technique gave satisfactory results. Unfortunately, nickel is relatively insensitive to this technique, and the detection limit for our crystals was on the order of 1000 ppm. Cobalt detection proved more sensitive, extending the limit to roughly 200 ppm. Since these levels were of the order of many of our doping concentrations, we were forced to estimate many of the concentrations. By analyzing linewidths, cavity loading, initial concentrations during the crystal growth process, and what nuclear-activation data were available, we feel the data on the weakest doping are accurate to within a factor of 2. It is quite improbable that any two samples presented in order of concentrations are, in fact, reversed. Great care was exercised in obtaining consistent data before the crystals were selected for inclusion in this report.

II. EXPERIMENTAL RESULTS

A. General

The EPR data of our pyrite single crystals were taken at 35 and 24 GHz using the spectrometers described in Sec. I. Because of the higher sensitivity of the 35-GHz unit (signal-to-noise ratio more than 10 dB greater), it was used for all parameter measurements. The 24-GHz device was used to confirm line assignments and to aid in determining parameters which could not be directly measured. Most measurements of the semiconductor $Ni_xFe_{1-x}S_2$ were taken at 77 °K. Whenever cobalt was introduced, the temperature was reduced to either 4 or 2 °K in an effort to freeze out the itinerant cobalt electrons. The normal operating range of the magnetic field was 0–13 kOe, with occasional sweeps up to 15 kOe. Since magnetic modulation was employed the spectrometer output displayed the first derivative of the absorption line shape.

B. System $Ni_xFe_{1-x}S_2$

The single-ion spectra of Ni^{2+}, diluted in the nonmagnetic insulating host FeS_2, was composed of four pairs of lines, each pair corresponding to one equivalent ⟨111⟩ axis. This spectrum, pictured in Fig. 1, can be fitted by a spin Hamiltonian of the form

$$H_s = g_z\mu_B H_z S_z + g_x\mu_B(H_x S_x + H_y S_y) + DS_z^2,$$

where $D = -1.21$ cm^{-1}, $g_z = 2.130 \pm 0.005$, $g_x = g_y = 2.110 \pm 0.005$, and $S = 1$. Figure 2 shows the energy-level diagram for this Hamiltonian for several different angles θ between the dc magnetic field and the axis of axial symmetry (any ⟨111⟩). For $\theta = 0$, the solid arrow represents the rf resonant energy

$$E/h = 35.05 \text{ GHz}$$

coupling an allowed ($\Delta M = \pm 1$) transition. The forbidden transition ($\Delta M = \pm 2$) is shown with a dashed line. The transition ($+1 \leftrightarrow 0$) remains at nearly constant intensity along its low-field position, falling off slightly with increasing angle as it begins to become forbidden. The ($+1 \leftrightarrow -1$) transition becomes comparable in size to ($+1 \leftrightarrow 0$) at large ($\theta \sim 50°$) angles but falls off rapidly as $\theta \to 0$ becoming strictly forbidden when H is oriented along the ⟨111⟩ axis. Linewidth increased monotonically with concentration x, changing dramatically at higher (3 at.%) concentrations as shown by the open circles in Fig. 3. Line intensity increased linearly with concentration indicating the absence of pairing at these dilute concentrations (Fig. 3). There was no evidence of pair lines at any concentration level. No hyperfine structure was present, as should be

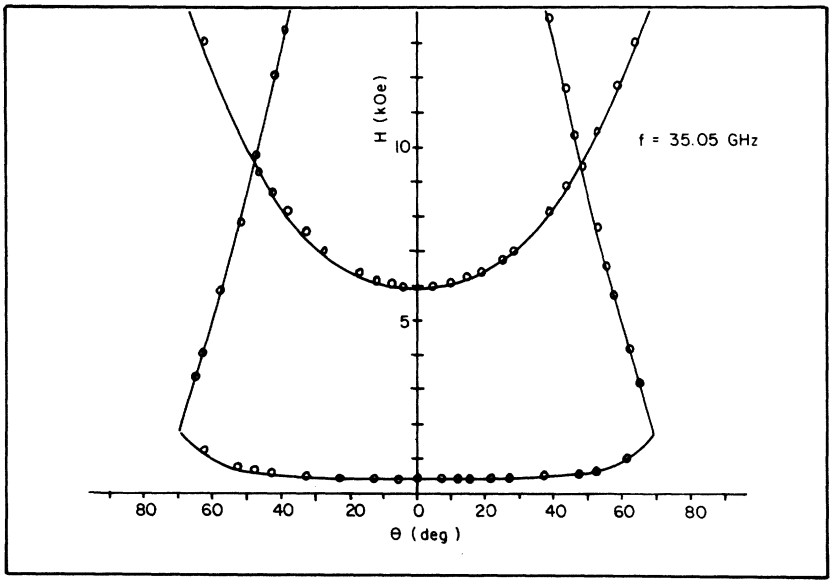

FIG. 1. θ dependence of the resonant H field for Ni^{2+} in FeS_2. The solid lines are a computer fit of the spin Hamiltonian in the text.

expected with the low natural abundance of Ni^{61}. There was some evidence of resistive loading of the microwave cavity, particularly for the heavier doped crystals. Asymmetry ratios (A/B as defined in Fig. 4) were low, equal to 1 for $x < 0.01$ and rising to 2 at $x = 0.03$. One sample, with $x = 0.023$, displayed an asymmetric line shape with $A/B = 2.3$, but was contaminated with chlorine.

C. System $Co_xFe_{1-x}S_2$

The solid solution $Co_xFe_{1-x}S_2$ exhibits semiconducting behavior at high frequencies only for $x < 50 \times 10^{-6}$. At $x = 100 \times 10^{-6}$ the crystal acts as a semimetal, loading the spectrometer even at coldest temperatures. The EPR spectra for the most dilute cases show an extremely broad ($\Delta H > 5$-kOe) line. For $x = 100 \times 10^{-6}$, where most electrons are

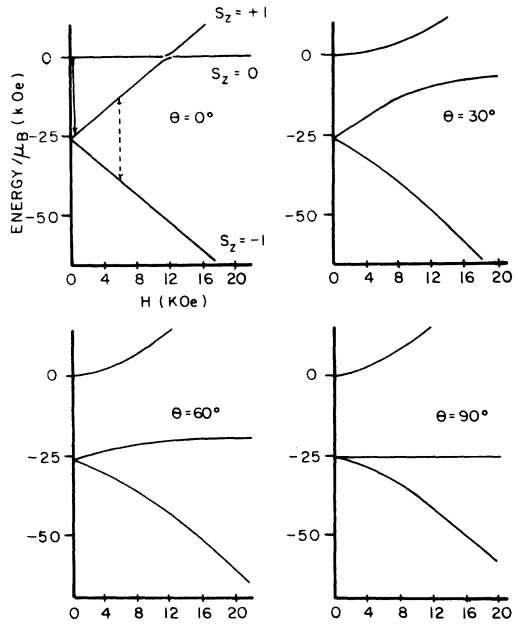

FIG. 2. Energy-level diagrams for Ni^{2+} in a pyrite structure. The resonant rf energy is shown as an arrow.

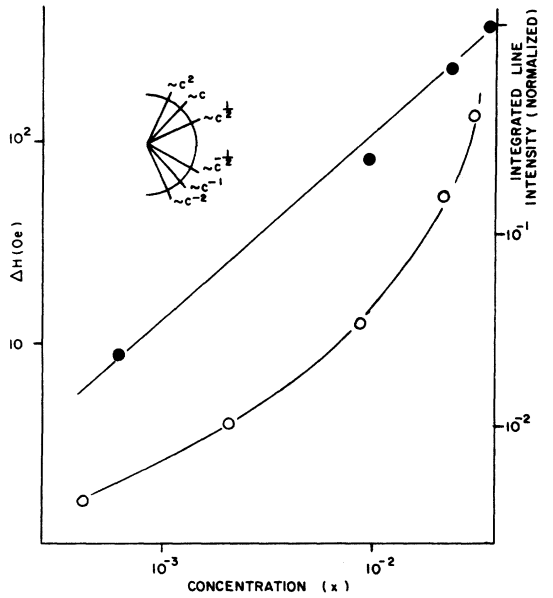

FIG. 3. Concentration dependence of the Ni^{2+} EPR linewidth (open circles) and line intensity (solid circles) for the system $Ni_xFe_{1-x}S_2$.

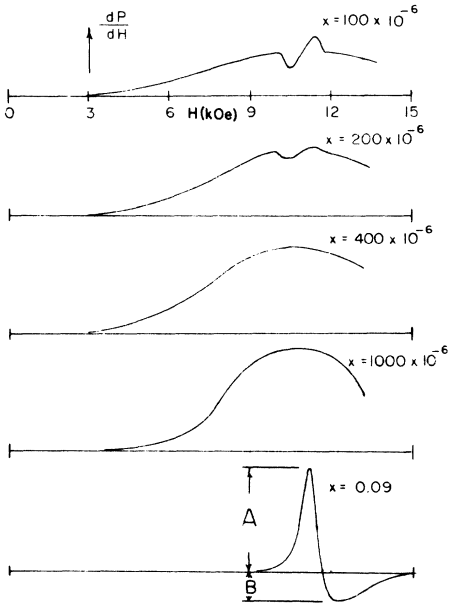

FIG. 4. Concentration dependence of the Co^{2+} EPR line shape for the system $Co_xFe_{1-x}S_2$.

localized at 4 °K, a narrower ($\Delta H = 900 \pm 50$-Oe) isotropic line appears at $g = 2.18 \pm 0.02$ in addition to the wide one. As T is reduced from 4 to 2 °K, the broader line weakens to roughly one-half its amplitude while the line at $g = 2.18$ remains at the same intensity. These lines are shown in Fig. 4. Decreasing x to 50×10^{-6} reduces the signal beyond the limits of detection, while raising the concentration of cobalt to $x = 400 \times 10^{-6}$ produces a semimetal requiring such severe decoupling that only the strong very broad line is detected. Further increasing of x to $x = 0.09$ results in a very strong well-defined line at $g = 2.12 \pm 0.01$. This line displays the classic asymmetric ($A/B = 2.8$) line shape described by Feher and Kip[8] as originating from a conduction electron. However, its limited motional narrowing ($\Delta H = 960 \pm 40$ Oe) and g value differentiate it from those motionally narrowed lines near $g = 2.0023$ normally encountered in conduction-electron spin-resonance experiments.

The endpoint $x = 1$ gives the metallic ferromagnet CoS_2. Because of the low magnetic anisotropy, the ferromagnetic resonance of this material is easily seen at 35 GHz. The line shape closely resembles the paramagnetic line shape for $x = 0.09$ shown in Fig. 4 with the exception of an increased linewidth ($\Delta H = 1200 \pm 50$ Oe) and the appearance of several smaller lines that are strongly θ dependent. These lines, which appear to be macroscopic magnetostatic modes due to field inhomogeneities (Walker modes), disappear as the sample is heated through the Curie temperature. The linewidth of this ferromagnetic crystal increases with temperature roughly as T^2.

D. System $Co_xNi_yFe_{1-x-y}S_2$

In addition to the two bication systems discussed, we also studied the system $Co_xNi_yFe_{1-x-y}S_2$ at low concentrations (x, $y < 0.004$). As was expected, both the four equivalent Ni^{2+} spectra characterized by $S = 1$ and the broad resonance associated with the itinerant cobalt e_g electrons appeared. At these levels of dilution, the nickel e_g electrons remain localized and have no effect on the broad cobalt spectra. The itinerant electrons, on the other hand, had a marked effect on the Ni^{2+} EPR line shape for both the $\Delta m = 1$ and $\Delta m = 2$ resonances. The sample $Co_{0.0001}Ni_{0.004}Fe_{0.9959}S_2$ is a semimetal with most of its electrons localized at 4 °K. The Ni^{2+} lineshape, shown in Fig. 5(a), displays a 2-Oe linewidth, as asymmetry ratio of 1.1, and a slight lip appearing on the high-field side. Holding y constant and increasing the cobalt concentration to $x = 500 \times 10^{-6}$, results in a nearly metallic crystal with little improvement in sample resistivity at coldest temperatures. The resulting Ni^{2+} line shape at constant input power level is shown in Fig. 5(b). When the cobalt concentration is now increased and the nickel concentration decreased so that $x = y = 1000 \times 10^{-6}$, the result is the asymmetric ($A/B = 0.75$) line shown in Fig. 5(c). At this concentration of cobalt, the sample was metallic and was decoupled to the bottom of the

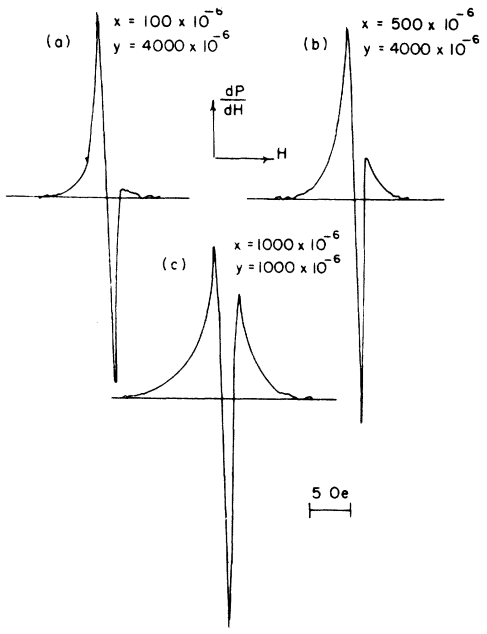

FIG. 5. Concentration dependence of the Ni^{2+} EPR line shape for the system $Co_xNi_yFe_{1-x-y}S_2$.

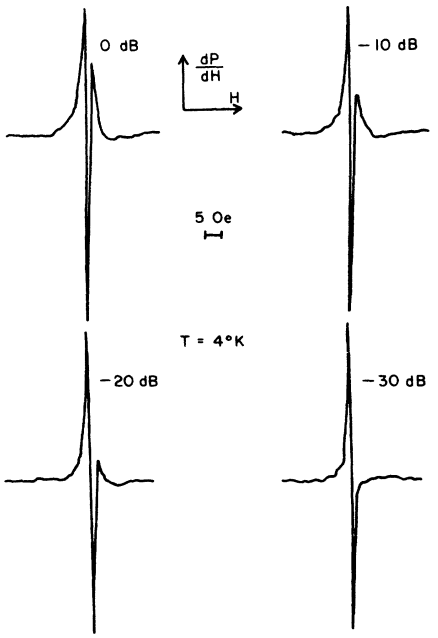

FIG. 6. EPR line shape of Ni^{2+} in $Co_{0.0005}Ni_{0.004}Fe_{0.9955}S_2$ as a function of input power level. All lines are normalized to unity peak-to-peak intensity.

cavity.

The semimetallic crystals all exhibited some power dependence of the line shape. A typical line shape development is shown in Fig. 6, where the linewidth remained constant but the asymmetry ratio varied from $A/B = 0.75$ to $A/B = 1.0$ over a 30-dB range of input power. In all cases shown, the line intensity scaled linearly with power level, indicating the presence of a relaxation mechanism efficient enough to prevent power saturation. The metallic samples did not exhibit this phenomenon.

III. THEORETICAL INTERPRETATION OF EXPERIMENTAL RESULTS

A. Paramagnetic-Antiferromagnetic System $Ni_xFe_{1-x}S_2$

1. Single-Ion Spectrum

Regardless of the strength of a cubic crystal field, divalent nickel lies in a $^3A_{2g}$ ionic ground state. This orbital singlet is not split by either a spin-orbit interaction or a trigonal distortion in the crystal field, but under the combined application of these operations does split into a singlet A_{1g} and a doublet E_g. This second-order splitting is small, usually 1 cm^{-1} or less. The Ni^{2+} is thus stabilized into an $S = 1$ ground state, which is exactly that obtained experimentally.

To be consistent with other transition metal ions in a cubic field with more than half-filled orbitals, one usually expects g to exceed the free-electron value of $g_e = 2.0023$. Since the g value for an orbital singlet is 2.0023 to first order, the additional contributions to g must come from second-order mixing of excited states into the ground state via the spin-orbit interaction.

In Appendix A we calculate the contribution of these excited states and conclude that only the state $^3T_{2g}$ couples significantly to the ground state through $\lambda\vec{L}\cdot\vec{S}$. This state contributes an amount $\Delta g = 0.126$ to the splitting factor to give $g_z = 2.128$, in excellent agreement with our measured value of $g_z = 2.130$.

The axial distortion parameter D is related to the g-value anisotropy $(g_z - g_x)$ in a complicated manner. In his thorough theoretical treatment of Cr^{3+} (d^3), MacFarlane[9–11] found D to be a linear function of the trigonal distortion parameters V and V^1, which are defined by the single-electron matrix elements

$$V = -3\langle t_{2g}|V_{trig}|t_{2g}\rangle,$$

$$V^1 = \langle e_g|V_{trig}|t_{2g}\rangle.$$

If we perform the same analysis for $(g_z - g_x)$ for the $^3A_{2g}$ ground state of Ni^{2+} in FeS_2, we find the same three perturbation graphs as in MacFarlane's Fig. 2 of Ref. 11 (with quartet states replaced by triplet states) contributing to the anisotropy. Likewise, if we neglect the contributions of the higher-lying $^1T_{2g}$ states, only graphs corresponding to (i) and (iii) in MacFarlane's Fig. 1 of Ref. 10 contribute in third order to the zero-field splitting D (again with quartet spin states replaced by triplet states). If we carry out the details of the perturbation calculation and use the fact that the spin Hamiltonian $D = -\frac{1}{2}$ times MacFarlane's $D(^3A_2)$ we get

$$D = (\lambda/6k)(g_z - g_x),$$

where k is the orbital reduction factor and λ is the free ion spin-orbit parameter.

For $k = 0.07$ and $\lambda_{Ni} = -325$ cm^{-1}, then $D = -1.3$ cm^{-1}, which agrees with the sign and magnitude of the measured parameter.

Line shape asymmetry ratios (A/B) are normally a result of itinerant electrons moving in and out of regions of high rf field. This effect is most pronounced in metals, where the fields are evanescent and the electrons have sufficient mobility such that the time spent within the skin depth T_D is short compared with their spin lifetime T_2. For impure semiconductors such as FeS_2 grown by chlorine transport, one can expect an anomalous skin effect where T_D and T_2 are comparable. Such a case results in reducing the asymmetry ratio from that found in "pure" metals $(A/B \simeq 30)$ by an order of magnitude. We can look upon CoS_2 as a high mobility limit for narrow band conduction and recall that, for all cases, $A/B \leq 3$. Thus, the in-

creasing asymmetry ratios found in $Ni_xFe_{1-x}S_2$ as x increases is interpreted as evidence of the delocalization of the Ni^{2+} e_g electrons and signaling the onset of collective electron behavior.

2. Collective Magnetic Effects—Narrow-Band Model

The predominately octahedral crystal field experienced by the transition-metal ion (T ion) splits the fivefold orbital degeneracy of the $3d$ band into an e_g doublet and a lower t_{2g} triplet. For sufficiently large splitting, the crystal-field potential will dominate over Hund's rule and the ion will stabilize in a low-spin configuration where the single-electron t_{2g} states are filled before electrons occupy the e_g levels. The anion S_2^{2-} complex, shown on the right-hand side of Fig. 7, forms four doubly degenerate sp^3 hybrid orbitals, one of which is split into occupied anion-anion bonding σ_A orbitals and empty antibonding σ_A^* orbitals. The remaining three orbitals interact covalently with the $e_g^2 sp^3$ cation orbitals to stabilize the predominately anionic orbitals and broaden them into covalent bonding σ bands. The cationic orbitals are destabilized by the same interaction and broadened to form antibonding σ^* bands. The t_{2g} cation orbitals are filled for the $3d^6$, $3d^7$, and $3d^8$ low-spin ions and remain localized and magnetically inactive around the cation. FeS_2, with a single-electron configuration t_{2g}^6, is therefore a nonmagnetic semiconductor. CoS_2, with a single e_g electron in the σ^* band, is metallic and ferromagnetic due to on-ion electronic correlation permitted by the narrowness of the band. NiS_2, with two e_g electrons, is a semiconductor by virtue of an interband splitting again due to narrow-band electronic correlation. In addition, exchange splitting may occur and dominate over the correlation energy, producing an antiferromagnet. The increasing linewidth and asymmetry ratios with x at these low concentrations is consistent with the concept of magnetic-moment delocalization within a macroscopically dilute magnetic sample.

B. Paramagnetic-Ferromagnetic System $Co_xFe_{1-x}S_2$

The system $Co_xFe_{1-x}S_2$ has been macroscopically studied by Jarret *et al.*[12] for $0.05 \leq x \leq 1.0$ and by others[13,14] at the limit points $x=0$ and $x=1$. The Co^{2+} ion is heavier than Fe^{2+} and can be expected to be lower in energy. Goodenough[15] extrapolated high-spin Co^{2+} and Fe^{2+} data from thiospinels to the low-spin case and estimated that the Co^{2+} $3d$ manifold lies 0.6 eV below that of FeS_2. Our ac data indicate that this figure is high. The semimetallic behavior at $x = 500\times10^{-6}$ implies that the cobalt e_g electrons initially enter the FeS_2 lattice as shallow donors within a few hundredths of an eV of the bottom of the FeS_2 antibonding σ^* band. At $x = 5000 \times10^{-6}$ the material is metallic with the very narrow cobalt σ^* band now completely overlapping the FeS_2 σ^* band.

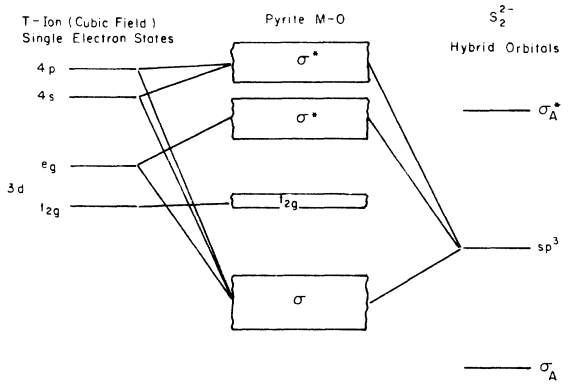

FIG. 7. Energy-level diagram for iron group disulfides in the pyrite structure.

1. Single-Ion Spectrum

Cobalt disulfide, as does the other pyrites studied, crystallizes in a low-spin state with a single-electron $t_{2g}^6 e_g^1$ configuration. The Co^{2+} ion, upon application of a cubic (or trigonal) crystal field, transforms into the ionic ground state ^2E_g. This orbital doublet has often been considered as a favorable state for the Jahn-Teller effect to be active. At low temperatures, this effect is usually manifested in a sizable distortion along the three equivalent cubic axes, producing an EPR spectrum consisting of three superimposed axial spectra. At higher temperatures the lattice distortions couple to the electronic ground state to form a vibronic ground state characterized by an isotropic EPR spectrum with an "averaged" g factor. Recently, however, there has been some evidence of this dynamic Jahn-Teller mechanism at coldest temperatures which originates in the zero-point ionic motion.[16]

A theoretical model for this low-temperature dynamic Jahn-Teller effect has been developed by Ham[17] for a ^2E_g electronic ground state. His results include a spin Hamiltonian, the non-isotropic terms of which are reduced by the application of any of the dynamic Jahn-Teller mechanisms. When random strains are introduced and dominate over the Zeeman terms, only the isotropic part of the Hamiltonian affects the g factor; the anisotropic part then serves as a line-broadening mechanism. Strong coupling of the ^2E_g state to the lattice can also produce a broad isotropic line by the strain coupling of the vibrational mode pair through the lattice distortion. Indeed, this strong coupling is consistent with the concept of small polaron formation that immediately precedes collective electron behavior in narrow bands. This isotropic spectrum should remain strong at coldest temperatures, as we observed experimentally. In addition, it seems plausible that an itinerant electron experiencing an

"average" g value from the three equivalent symmetry axes can produce an isotropic motionally broadened spectrum. Such a model would be consistent with our finding of no hyperfine structure in the data. In all three cases the isotropic resonance is given by $g=g_1$, the same value that would result from a ^2E_g ground state in full cubic symmetry. In Appendix B we calculate this g factor to be $g=2.16$ in good agreement with the measured value of $g=2.18\pm0.02$.

2. Collective Phenomena

Increasing the cobalt concentration to $x=0.09$ results in metallic conduction within the narrow cobalt σ^* band and perhaps the narrowing iron σ^* band as well. As was mentioned earlier, the paramagnetic-resonance spectrum produced an isotropic line at $g=2.12\pm0.01$ displaying the classic conduction-electron line shape. The asymmetry ratio was given by $A/B\leq 3.0$ with roll off on the high-field side. The g value reflects a stronger coupling to the lattice than is encountered in wide-band electrons, a result consistent with the concept of narrow bands. Fredkin and Freedman, [18] in a recent theoretical paper on g-factor anisotropy in metals, concluded that the combined presence of such anisotropy and electron correlation effects resulted in a shift of the collective resonance toward higher g values. Furthermore, a reduction in electron correlation while the anisotropy still existed resulted in an extremely broad line. Since donor electrons in the iron disulfide σ^* band are expected to be weakly correlated, it is not unexpected that they should be responsible for the very broad line occurring at semimetallic concentrations.

The observed asymmetry ratio of $A/B\leq 3$ for $x\geq 0.09$ is consistent with the concept of a conduction electron of limited mobility and is interpreted as a high-mobility limit for narrow-band conduction.

C. Dilute Paramagnetic System $Co_xNi_yFe_{1-x-y}S_2$

1. Theory of s-d Interactions

The first model for s-d interactions was developed by Hasegawa[19] to explain the absence of an expected g shift and line broadening of the magnetic impurity Mn in Cu. Hasegawa considered a binary system of the impurity magnetization M_d and the conduction-electron magnetization M_s and included, in addition to the lattice relaxation parameters T_{sl} and T_{dl}, the possibility of cross relaxation via T_{sd} and T_{ds}. T_{ds}, the impurity-to-conduction-electron relaxation time, is related to T_{sd} by a detailed balanced equation

$$T_{sd}\chi_d^0 = T_{ds}\chi_s^0,$$

where χ_d^0 and χ_s^0 are the susceptibilities of the impurity and conduction-electron systems, respectively, for noninteracting systems. Hasegawa argued that for a favorable ratio of these susceptibilities,

$$\chi_r^0=\chi_d^0/\chi_s^0,$$

the systems would be crossrelaxed, that is, as M_d relaxed to M_s via T_{ds}, the energy did not dump into the lattice via T_{sl} but was returned to M_d via T_{sd}. This situation, which he described as "bottlenecked," effectively removed the spin system as a relaxation mechanism and hence reduced its effect on line broadening and g shifts.

Hasegawa explained his model by using phenomenological Bloch-type equations that were coupled through the cross-relaxation terms and the exchange fields. Recently, several other authors[20–22] have refined and extended these equations with the intention of applying the results to transmission electron spin resonance (TESR). Pifer and Longo[22] (PL) treat the problem more generally by considering the conduction electrons on an equal footing with the magnetic impurity electrons rather than as a vehicle for impurity relaxation.

Among several regimes covered in their analysis, PL consider the case of constant negative exchange and varying susceptibility ratios χ_r^0. For such a system, the line shape displays the following characteristics: (i) For large χ_r^0 the line shape is essentially d-like with small asymmetry ratios (A/B) and a lip on the high-field side. (ii) As χ_r^0 is reduced, the line loses its d character; the high-field lip intensifies and the low-field side broadens as it absorbs s character. (iii) The low-field lip intensity and s character of the hybrid line are strong functions of the drift current and disappear rapidly as the sample conductivity decreases.

2. Application of s-d Interaction Theory to the Ni^{2+} Line Shape in $Co_xNi_yFe_{1-x-y}S_2$

The system $Co_{0.0001}Ni_{0.004}Fe_{0.9959}S_2$ can be expected to have the highest χ_r^0 of the three systems reported ($y/x=40$). The line shape, shown in Fig. 5, is identical to that described by PL for negative exchange and large χ_r^0 (the Ni^{2+} ions couple antiferromagnetically to the itinerant cobalt e_g electrons). As we increase x, PL predict the high-field lip to intensify and the low-field side to broaden, which we observe experimentally. The dependence of the line shape on power for the sample $Co_{0.0005}Ni_{0.004}Fe_{0.9955}S_2$ is not completely understood. Two possibilities are (a) that the rf power is exciting electrons over the density-of-states minimum and thereby increasing the sample conductivity, or (b) that the coupled nature of the system is not observable unless excess rf power requires the need for a $d\rightarrow s$ relaxation mechanism. Neither of the above possibilities has been subjected to ex-

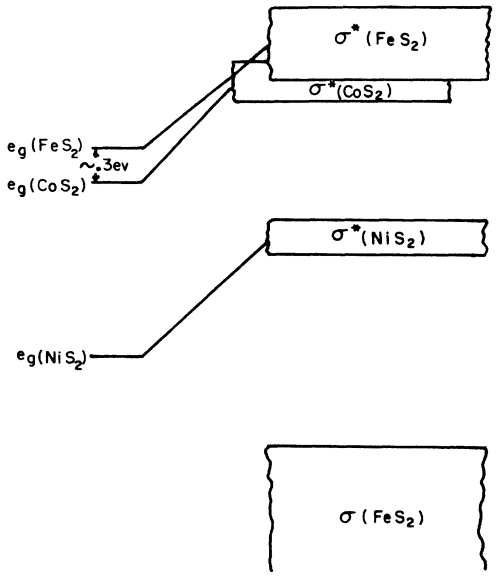

FIG. 8. Proposed partial energy-band scheme for Co^{2+} and Ni^{2+} impurities in FeS_2.

perimental (or theoretical) justification at this point.

The final sample, $Co_{0.001}Ni_{0.001}Fe_{0.998}S_2$, probably has the lowest χ_r^0 of the three ($y/x \simeq 1$). It displays the largest high-field lip and widest low-field skirt consistent with the theory. Furthermore, as a metal, the insensitivity of its lineshape to power level is consistent, if our proposition (a) above is credible.

IV. CONCLUSIONS

Although not conclusive in all respects, our results are consistent with the following description of bands and energy levels in these materials. For the system $Ni_xFe_{1-x}S_2$, we conclude that the nickel e_g electrons initially enter the host lattice as very deep donors, as shown in Fig. 8. The Ni^{2+} ions are thus stabilized in a localized $S=1$ spin state for dilute cases ($x < 0.002$). As the concentration increases toward $x = 0.03$, the increasing NiS_2 σ^* bandwidth results in some delocalization of the e_g electrons as evidenced by the increase in asymmetry ratio. Because of the large energy separation between the very narrow NiS_2 σ^* band and the FeS_2 σ^* band, donor electrons are not excited up as uncorrelated carriers, but rather delocalize within their own narrow σ^* band, always remaining correlated.

On the other hand, for the system $Co_xFe_{1-x}S_2$, the cobalt e_g electrons initially enter the host lattice as very shallow donors within a few hundredths of an eV of the bottom of the FeS_2 σ^* antibonding level, forming localized ^2E_g states complicated by a dynamic Jahn-Teller mechanism. At $x = 0.0005$, the very narrow CoS_2 σ^* band is broad enough to just overlap the FeS_2 σ^* band (Fig. 8) creating a density-of-states minimum near the Fermi level. As x continues to increase, the density-of-states minimum vanishes and uncorrelated electron conduction occurs within the overlapped band. Continued increasing of x results in an increase in the number of σ^* electrons which increases the correlation of these electrons until, at $x \simeq 0.10$, the conduction mechanism is primarily that of correlated electrons within the combined FeS_2-CoS_2 σ^* band. This transition to a correlated conduction regime is also marked by the onset of ferromagnetic order, as verified by our own pyromagnetic magnetometer studies and the previous work of Jarret *et al.*[12] Of the samples discussed, $Co_xFe_{1-x}S_2$ for $x \geq 0.10$ present the most graphic examples of narrow-band behavior. The characteristics of collective behavior (metallic conduction, asymmetry ratios >2.8) occur simultaneously with characteristics of localized behavior (large g value, magnetic order). Furthermore, the limited motional narrowing of the paramagnetic resonance line is consistent with the concept of reduced electron mobility within a narrow conduction band.

APPENDIX A: g VALUE FOR Ni^{2+} IN A $^3A_{2g}$ GROUND STATE

The parallel g values are defined by the expectation of the Zeeman Hamiltonian

$$\langle \psi_m | (L_z + g_e S_z) \mu_B H_z | \psi_m \rangle = g_z \mu_B H, \tag{A1}$$

where ψ_m is the ionic ground state of appropriate crystal-field symmetry corrected to first order in spin orbit, i.e.,

$$\psi_m = \psi_0 - \sum_k \psi_k \frac{\langle k | \lambda \vec{L} \cdot \vec{S} | 0 \rangle}{E_k - E_0}, \tag{A2}$$

where ψ_0 is the unperturbed crystal-field ground state with energy E_0. Taking the expectation of H_z with respect to the new ground state gives, for $H = H_z$,

$$\langle m | (L_z + g_e S_z) \mu_B H | m \rangle = \langle 0 | L_z + g_e S_z | 0 \rangle \mu_B H_z - \sum_k \langle 0 | \mu_B H_z \frac{L_z + g_e S_z}{E_k - E_0} | k \rangle \langle k | \lambda \vec{L} \cdot \vec{S} | 0 \rangle + \text{higher-order terms}. \tag{A3}$$

By identifying the first term as $g_e \mu_B H_z$ for a singlet ground state, we get, for $|0\rangle = |^3A_{2g}\rangle$,

$$\langle m | H_{\text{Zeeman}} | m \rangle = g_e \mu_B H_z - \lambda \sum_k \langle {}^3A_{2g} | \frac{\mu_B H_z (L_z + g_e S_z)}{E_k - E_0} | k \rangle \langle k | \vec{L} \cdot \vec{S} | {}^3A_{2g} \rangle .$$

But since a nonvanishing $\langle {}^3A_{2g} | S_z H_z | k \rangle$ requires $|k\rangle$ to have A_{2g} orbital symmetry the entire term

$$\langle {}^3A_{2g}| \frac{S_g H_g}{E_k - E_0} |k\rangle\langle k|\vec{L}\cdot\vec{S}|{}^3A_{2g}\rangle$$

must vanish by virtue of

$$\frac{\langle A_{2g}|\vec{L}\cdot\vec{S}|A_{2g}\rangle}{E_k - E_0} = 0$$

which leaves us with only the orbital part of the Zeeman operator. Thus

$$\langle m|H_g|m\rangle = g_e\mu_B H - \lambda\sum_k \frac{\langle {}^3A_{2g}|L_g\mu_B H|k\rangle\langle k|\vec{L}\cdot\vec{S}|{}^3A_{2g}\rangle}{E_k - E_0}.$$

Since the orbital Zeeman operator does not operate on the spin of $|k\rangle$, $|k\rangle$ must be a spin triplet. Within 10^5 cm^{-1} of E_0 there are only two excited spin triplets; ${}^3T_{2g}$ and ${}^3T_{1g}$, both of which originate from an excited $(t_{2g}^5 e_g^3)$ configuration. From group theoretical considerations, only the ${}^3T_{2g}$ mixes into the ${}^3A_{2g}$ state via the spin-orbit interactions, and it alone should account for all of the second order corrections to g. Therefore, in general,

$$\Delta g = g - 2.0023 = -\frac{\lambda\langle {}^3A_{2g}|\vec{L}\cdot\vec{H}|{}^3T_{2g}\rangle\langle {}^3T_{2g}|\vec{L}\cdot\vec{S}|{}^3A_{2g}\rangle}{\Delta},$$

where $\Delta = E({}^3T_{2g}) - E_0$.

This particular perturbational coupling is found in the literature[9] and is given as

$$\Delta g = -8\lambda/\Delta . \qquad \text{(A4)}$$

To calculate Δ, note that the criterion for a low-spin configuration in FeS_2 is $10Dq \geq 2$ eV.[23] We can expect the $10Dq$ splitting to increase for Ni^{2+} by roughly the ratio of the fourth power of the unit-cell dimension a for FeS_2 and NiS_2. Hence, for Ni^{2+},

$$10Dq_{Ni} \sim 10Dq_{Fe}[a_{Ni}/a_{Fe}]^4 = 20\,300\ cm^{-1}.$$

With this splitting, Tanabe and Sugano[23] give the ${}^3T_{2g}$ level as 20 600 cm^{-1} above the ground state ${}^3A_{2g}$. Thus, with the free-ion value of $\lambda_{Ni} = -324$ cm^{-1}, $\Delta g \leq 0.126$, $g \leq 2.128$.

APPENDIX B: g VALUE FOR Co^{2+} IN A ${}^2E_g$ GROUND STATE

As in Appendix A, we need to calculate the expectation

$$\langle m|L_z + g_e S_z|m\rangle , \qquad \text{(B1)}$$

where, as before, $|m\rangle$ is the ground state correct to first order in $\lambda\vec{L}\cdot\vec{S}$. However, since the unperturbed ground state is orbitally degenerate, we need to evaluate the orbital Zeeman term within this manifold:

$$\langle 0|\vec{H}\cdot\vec{L}|0\rangle = \langle E_g|\vec{H}\cdot\vec{L}|E_g\rangle . \qquad \text{(B2)}$$

L transforms under the irreducible representation T_{1g}. Since the direct product $T_{1g}\times E_g$ does not contain E_g, the matrix element (B2) must vanish. By explicitly removing this element from consideration in calculating (B1), we can directly apply the results of Appendix A without concern over contributions within the degenerate manifold. We obtain

$$\Delta g = \sum_k \frac{\langle {}^2E_g|\vec{H}\cdot\vec{L}|k\rangle\langle k|\vec{L}\cdot\vec{S}|{}^2E_g\rangle}{E_k - E_0},$$

where E_0 is the energy of the unperturbed manifold ${}^2E_g$. The spin operator S also transforms under the irreducible representation T_{1g}. Since $T_{1g}(\Gamma_4)\times\Gamma_4$ contains only the spin doublet Γ_6 and the spin quartet Γ_8, while $T_{1g}(\Gamma_4)\times E_g(\Gamma_3)$ contains only the orbital triplets T_{1g} and T_{2g}, $|k\rangle$ can only assume the symmetries of ${}^2T_{1g}$, ${}^4T_{1g}$, ${}^2T_{2g}$, or ${}^4T_{2g}$ for a nonvanishing matrix element

$$\langle k|\lambda\vec{L}\cdot\vec{S}|{}^2E_{2g}\rangle .$$

Furthermore, since the orbital Zeeman term does not operate on spin, the only states among the four to survive the nonvanishing element

$$\langle k|\vec{H}\cdot\vec{L}|{}^2E_g\rangle$$

are the spin doublets ${}^2T_{1g}$ and ${}^2T_{2g}$. Thus, from Appendix A,

$$g = g_e - 8\lambda\left(\frac{1}{\Delta^2 T_{1g}} + \frac{1}{\Delta^2 T_{2g}}\right).$$

The nearest states of correct symmetry are the nearly degenerate pair originating in the excited $(t_{2g}^5 e_g^2)$ configuration. We estimate these states to lie over 17 800 cm^{-1} above the ground state. Thus, for the free Co^{2+} ion value of $\lambda = -180$ cm^{-1}, $\Delta g \leq 0.162$, $g \leq 2.164$.

---

†Based upon a Ph.D. dissertation by R. N. Chandler, University of Texas, 1972; supported principally by the Joint Services Electronics Program under Research Grant No. AF-AFOSR-69-1972A.

*Present address: Schlumberger Well Services, P. O. Box 2175, Houston, Tex. 77001.

[1]J. Hubbard, Proc. R. Soc. A **276**, 238 (1963).
[2]J. Hubbard, Proc. R. Soc. A **281**, 401 (1964).
[3]R. Kishore and S. K. Joshi, Phys. Rev. **186**, 484 (1969).
[4]R. A. Bari, D. Adler, and R. V. Lange, Phys. Rev. B **4**, 3797 (1971).
[5]T. Arai, Phys. Rev. B **4**, 216 (1971).
[6]L. G. Caron and G. Kemeny, Phys. Rev. B **3**, 3007 (1971).
[7]R. J. Bouchard, J. Cryst. Growth **2**, 39 (1968).
[8]G. Feher and A. F. Kip, Phys. Rev. **98**, 337 (1955).
[9]R. M. MacFarlane, J. Chem. Phys. **39**, 3118 (1963).
[10]R. M. MacFarlane, J. Chem. Phys. **47**, 2066 (1967).
[11]R. M. MacFarlane, Phys. Rev. B **1**, 989 (1970).
[12]H. S. Jarret, W. H. Cloud, R. J. Bouchard, S. R. Butler, C. G. Frederick, and J. L. Gillison, Phys. Rev. Lett. **21**, 617 (1968).
[13]S. Furuseth and A. Kjekshus, Acta Chem. Scand. **23**, 8 (1969).
[14]A. K. L. Fan, Ph.D. thesis (Brown University, 1972) (unpublished).
[15]J. B. Goodenough, J. Solid State Chem. **3**, 26 (1971).
[16]R. E. Coffman, Phys. Lett. **21**, 381 (1966).
[17]F. S. Ham, Phys. Rev. **166**, 307 (1968).

[18]D. R. Fredkin and R. Freedman, Phys. Rev. Lett. **29**, 1390 (1972).
[19]H. Hasegawa, Prog. Theor. Phys. **21**, 483 (1959).
[20]D. C. Langreth, D. L. Cowan, and J. W. Wilkins, Solid State Commun. **6**, 131 (1968).
[21]D. C. Langreth and J. W. Wilkins, *Theory of Spin Resonance in Dilute Magnetic Alloys* (Rutgers U. P. New Brunswick, N. N. J., 1970), Vol. I.
[22]J. H. Pifer and R. T. Longo, Phys. Rev. B **4**, 3797 (1971).
[23]Y. Tanabe and S. Sugano, J. Phys. Soc. Jap. **9**, 753 (1950).